Cancer Biol Med 2025. doi: 10.20892/j.issn.2095-3941.2024.0297

ORIGINAL ARTICLE

The polarity protein Par3 enhances renal cell carcinoma metastasis *via* YAP/TAZ activation

Soo Lee[1], Jonathan Balcazar[1], Karla Davis[1], Rey-Chen Pong[1], Jer-Tsong Hsieh[1], Payal Kapur[2], Xiaosong Meng[1]
[1]Department of Urology, University of Texas Southwestern Medical Center, Dallas, TX 75390, USA; [2]Department of Pathology, University of Texas Southwestern Medical Center, Dallas, TX 75390, USA

ABSTRACT

Objective: Partitioning defective protein 3 (Par3) has recently been found to have important roles in cancer progression. Interestingly, Par3's functions vary among cancers: both Par3 elevation (in the prostate or liver) and loss (in the breast or lung) have been implicated in cancer metastasis. Although Par3 overexpression has been correlated with diminished survival in renal cell carcinoma (RCC), data indicating the role of Par3 in RCC metastasis are lacking. Given reports of interactions between Par3 and oncoproteins such as Yes-associated protein (YAP)/WW domain-containing transcription regulator 1 (TAZ), we investigated whether Par3-mediated RCC metastasis might be due to activation of the Hippo pathway components YAP and TAZ.

Methods: Par3 levels were analyzed in RCC cell lines and human RCC patient tissues by western blotting and immunohistochemical (IHC) staining, as appropriate. Co-immunoprecipitation (co-IP) and immunofluorescence studies were conducted to examine the interaction between Par3 and YAP. Quantitative PCR and luciferase assays were used to investigate the effects of Par3 on YAP target gene expression and co-transcriptional regulation. PDZ domain deletion mutants of Par3 were generated to elucidate the structural basis of the interaction between Par3 and YAP.

Results: Higher Par3 levels were found in distant-organ-RCC-metastasis-derived ACHN sublines than wild type ACHN cell lines. Par3 levels were also higher in the patient tissue obtained from metastatic sites than in normal kidney and primary RCC tumor tissues. Co-IP and IHC experiments demonstrated that Par3 directly interacted and co-localized with YAP/TAZ proteins. Moreover, Par3 upregulated the transcription of YAP/TAZ downstream target genes and increased the luciferase activity of YAP/TAZ responsive elements. PDZ domain 3 in the *PARD3* gene was demonstrated to be particularly important in the interactions between Par3 and YAP. Furthermore, Par3 was found to upregulate intracellular levels of YAP/TAZ molecules and promote nuclear translocation of YAP.

Conclusions: Together, these results indicate the role of Par3 in RCC metastasis, *via* driving metastatic RCC progression by promoting the YAP/TAZ pathway.

KEYWORDS Renal cell carcinoma (RCC); Par3; YAP; metastasis

Introduction

Polarity protein complexes are critical in maintaining epithelial apical–basal polarity in normal cells[1]. The core polarity protein members include the partitioning protein (Par) complex, comprising atypical protein kinase C (aPKC), Par3, Par6, and Cdc42-GTP[2,3]. However, the normal polarity regulatory function of the Par complex is lost in tumor formation and cancer progression, and is frequently assumed to be a common feature of cancer progression[4].

Par3 is encoded by the *PARD3* gene, which is evolutionarily conserved across species. Par3 contains a conserved N terminus and 3 PDZ domains (also known as Discs-large homologous regions or GLGF). Several Par3 isoforms (of 180 kDa, 150 kDa, and 100 kDa) are formed through alternative splicing of the *PARD3* gene, and multiple variants are often simultaneously expressed within a given cell type or tissue[5]. The 3 isoforms share a common N-terminal region and 3 PDZ domains, but the 100 kDa isoform lacks the aPKC binding site[6]. Par3 is phosphorylated by aPKCζ/ι and Par1[7]. Furthermore, Par3 is dephosphorylated by serine/threonine protein phosphatase PP1 (predominantly the α form)[7].

Correspondence to: Xiaosong Meng
E-mail: xiaosong.meng@utsouthwestern.edu
ORCID ID: https://orcid.org/0000-0003-1120-7691
Received July 23, 2024; accepted February 4, 2025;
published online July 8, 2025.
Available at www.cancerbiomed.org
©2025 The Authors. Creative Commons Attribution-NonCommercial 4.0 International License

Wu et al.[8] have demonstrated how Par3 regulates phosphoinositide signaling during the cellular polarization process. However, Par3 has been reported to control different signaling pathways in cancer cells. Zhou et al.[9] have shown that elevated Par3 expression inactivates the Hippo pathway in prostate cancer cells, and Zhang et al.[10] have revealed that downregulation of Par3 potentiates TGF-β1-induced epithelial-to-mesenchymal transition and activation of Tiam1-Rac1 signaling in thyroid cancer cells. Furthermore, depletion of Par3 increases lung cancer metastasis[11], whereas overexpression (OE) of Par3 decreases pancreatic cancer metastasis[12]; both effects have been shown to be associated with Par3 regulation of the TIAM/RAC1 signaling pathway.

Par3's role in tumorigenesis has been studied in many types of cancers. Whether Par3 promotes or inhibits tumorigenesis is controversial, given that the results vary by cancer type. In breast[13] and prostate[14] cancers, loss of Par3 has been reported to promote tumorigenesis by accelerating cell growth and division. In contrast, elevated Par3 expression correlates with poor prognosis in ovarian cancer[15] and hepatocarcinoma[16]. Hence, a dual role of Par3 in tumorigenesis has been suggested[17].

The role of Par3 in metastasis also varies among cancer types. Whereas elevated levels of Par3 have been suggested to promote metastasis in prostate cancer[9], colorectal cancer[18], and hepatocarcinoma[19], loss of Par3 appears to promote metastasis in breast cancer[20], bladder cancer[21], glioblastoma[22], and lung cancer[11]. To date, the role of Par3 in renal cell carcinoma (RCC) metastasis has not been extensively studied, although a correlation between Par3 OE and diminished survival has been reported[23].

Yes-associated protein (YAP) and its partner WW domain-containing transcription regulator 1 (TAZ) are key members of the Hippo pathway. YAP and TAZ have been identified as oncoproteins, and elevated YAP expression has been observed in various cancers[24,25]. Consequently, these proteins have been suggested to be primary mediators of metastatic progression[26,27].

Interestingly, Par3 co-localizes with YAP in the nuclei in proliferating canine kidney MDCK cells[28]. Nuclear-cytoplasmic translocation of YAP under various physiological and pathological conditions has been reported[29,30]. YAP has been suggested to translocate to the nucleus and subsequently drive gene transcription associated with proliferation and metastasis when the Hippo pathway is "off"; however, its subcellular location is restricted to the cytoplasm when the Hippo pathway is "on"[31]. Phosphorylation by the LATS (Warts homologs) tumor suppressor kinase leads to cytoplasmic translocation and inactivation of YAP[32]. The YAP/TAZ complex interacts with the transcriptional enhancer associated domain transcription factors (TEAD1–4), thus promoting the expression of proliferation- and metastasis-associated molecules[33].

Whether nuclear Par3 interacts with YAP and subsequently influences cancer metastasis has not been studied to date. Herein, we focused on exploring the role of nuclear Par3 as a cofactor for YAP/TAZ activation that promotes RCC metastasis.

Materials and methods

Cell lines

Human Caki-1 (clear cell) and ACHN (papillary) RCC cell lines were purchased from the American Type Culture Collection (ATCC, Manassas, VA). ACHN wild type (WT) and its metastasized organ-derived cell lines were as previously described[34,35]. HEK293T WT and Lenti X-HEK293 cell lines were also obtained from the ATCC. All RCC cells were cultured in RPMI1640 containing 10% FBS and 1× penicillin/streptomycin, and HEK293 cell lines were grown in DMEM containing 10% FBS and 1× penicillin/streptomycin. All cells were maintained in a humidified 5% CO_2 environment at 37°C.

Creation of cell lines with Par3 overexpression or knockdown

Transient transfection of siRNA-Par3 (Invitrogen, ID 132893, Cat no. AM16708) or negative scrambled (sc) siRNA control plasmid (Cat no. 462001) was performed with Lipofectamine3000 (Invitrogen) or Xfect (Takara Bio, San Jose, CA), and cells were harvested 24–48 h after transfection.

EGFP-tagged mouse full-length Par3 (FL-Par3) and Par3 mutant forms with deleted PDZ domains (domain 1 deleted, Δ1-Par3; domain 2 deleted, Δ2-Par3; domain 3 deleted, Δ3-Par3; and domain 1/3 deleted, Δ1/3-Par3) were constructed in the pEGFP-C2 vector[36]. Cell extracts/total RNAs were obtained and used in IP/luciferase experiments 24–96 h after transient transfection.

To create clone cell lines with stable Par3 knockdown (KD), we mixed shRNA-Par3 (Origene, TR302678, retroviral vector)

or sc control plasmid (Origene, TR30012) with psPAX2 and pMD2G in a 4:3:1 ratio to generate lentivirus in Lenti X-HEK293 cells. Subsequently, RCC cells were infected with viral supernatants (with polybrene, 6 μg/mL), and positive cells were selected with puromycin (0.5 μg/mL). Caki-1-derived cells with stable OE of Par3 or vector control were obtained similarly through transfection of cells with the pEGFP-C2 vector containing full-length Par3, which were selected with gradually increasing concentrations of G418 (200–800 μg/mL). After selection of individual clones, Par3 KD or OE cell lines were subjected to western blotting or quantitative PCR (qPCR) analyses to confirm Par3 levels.

Transwell migration and invasion assays

Migration assays were performed with Transwell chambers (8 μm pore size, Corning, Glendale, AZ). Cells (1×10^4 to 5×10^4) were plated into the upper chamber in serum-free RPMI culture medium (100 μL). A total of 700 μL of RPMI culture medium with 20% FBS was added into the lower chamber as the chemoattractant, and cells were incubated for 24 h. For invasion assays, membranes were pre-coated with 50 μL of 1:6 Matrigel:medium. Cells were seeded at 1×10^5 and incubated 48 h. After incubation, cells were fixed with methanol for 15 min, then stained with 0.2% crystal violet in 20% methanol. Cells that had migrated or invaded the lower chamber were photographed with a Keyence BZ-X710 microscope. For quantification of cell migration/invasion, crystal violet stain was extracted with 300 μL of 10% acetic acid, and the absorbance was measured at 570 nm wavelength with an Epoch microplate spectrophotometer (Agilent Technologies Inc., Santa Clara, CA).

Luciferase assays

Luciferase assays were performed with the YAP/TAZ reporter 8xGTIIC-lux. Either Par3 expression vector or siRNA-Par3 was co-transfected with the luciferase reporter (50 ng/cm^2) into cells (2×10^5 cells in 24 well plates) that were harvested 24 h after transfection. Luciferase activity was detected with a luminometer (Turner Biosystems, Sunnyvale, CA) and luciferase activity kit (Promega, Madison, WI). Luciferase specific activity was normalized to the protein concentration in each well. Each group was assayed in triplicate, and the entire experiment was repeated at least 3 times.

Immunofluorescence staining

Cells (1×10^4) were mounted on chamber slides (MilliCell EX slide, EMD Millipore, Temecula, CA), fixed, and stained with antibodies to Par3 (07-330, EMD Millipore) (1:200) and YAP (sc-101199, Santa Cruz, Santa Cruz, CA) (1:200). Cy5 tagged goat anti-rabbit (A10523), anti-mouse (A10524), and Alexa Fluor 488 tagged goat anti-mouse (A11001), and anti-rabbit (A11002) secondary antibodies (Invitrogen) (1:1000), were subsequently added. Immunofluorescence (IF) images were obtained with a fluorescence microscope (model BZ-X710, Keyence, Plano TX).

Cell protein extraction and western blot analysis

To obtain total cell extracts, we lysed cells in RIPA buffer (50 mM Tris-Cl, pH 7.5, 150 mM NaCl, 1% NP-40, 0.5% sodium deoxycholate, 1 mM EDTA, 1 μg/mL leupeptin, 1 μg/mL aprotinin, and 0.2 mM PMSF). To obtain cytoplasmic, membrane, and nuclear fractions, we used a Subcellular Protein Fractionation kit (Cat no. 78840, Thermo Fisher Scientific, Waltham, MA). Cells were harvested, incubated with cytoplasmic extraction buffer, membrane extraction buffer, and nuclear extraction buffer, in a stepwise manner, according to the manufacturer's instructions (Fisher). Cell extracts (total, 20–40 μg; subcellular fraction, 10–20 μg) were separated on 4%–12% Tris-Glycine SDS/PAGE gels (Bio-Rad), then transferred to PVDF membranes (162-0177, Bio-Rad). After being blocked in 5% non-fat dry milk, the membranes were incubated with primary antibodies (abs) at the manufacturers' suggested dilutions. Abs to the following targets were used: E-cad (3195T), CYR61 (14479T), and ANKRD15 (69953S) from Cell Signaling Technologies (Danvers, MA); actin (sc-58673), GAPDH (sc-166574), YAP (sc-101199), and CTGF (sc-373936) from Santa Cruz (Santa Cruz, CA); p-NF-κB (MAB7226) from R&D system (Minneapolis, MN); Par3 (NBP1-88861), FAK (NBP2-67327), N-cad (NBP1-48309SS), MMP2 (NB200-114SS), and GFP (NB600-597) from Novus; TGF-β1 (A18692) from Abcam Inc. (Cambridge, MA); vimentin (GTX100619), smad4 (GTX112980), and LDHA (GTX101416) from Gentex Inc. (Irvine, CA); p-YAP (Ser127, MBS9601097) from My BioSource (San Diego, CA); AREG (Amphiregulin) (bs-3847R-TR) from Bioss (Woburn, MA); NMP P84 (A8179) from ABclonal (Woburn, MA); and TAZ

(WWTR1) (66500-1-Ig) from ProteinTech (Rosemont, IL). Membranes were then incubated with HRP-conjugated secondary antibodies [1:3000, 170-6516 (mouse) and 170-6515 (rabbit), Bio-Rad], and protein bands were visualized with an Alpha Innotech Imager (Biocompare, San Francisco, CA) with ECL developing reagents (Advansta Inc., San Jose, CA) from Cell Signaling Technology.

qPCR analysis

Total cellular RNA extract was prepared with a Maxwell® 16 LEV Simply RNA Cell Kit (Promega, Madison, WI), and 2 μg RNA was reverse transcribed with Superscript III transcriptase (Invitrogen, Carlsbad, CA). qPCR analyses were conducted with specific primers (sequences in **Table S1**) mixed with SYBR® Green master mix (Bio-Rad) in a Bio-Rad CFX96 system, to determine the mRNA expression levels of the gene of interest. Expression levels were normalized to 18S mRNA levels.

Co-immunoprecipitation (co-IP)

Co-IP, Dynabeads™ Protein G (Invitrogen) (50 μL per reaction) were incubated with abs to either Par3 (NBP-1-88861, Novus) (1:100) or YAP (sc-101199, Santa Cruz) (1:200). Excess abs were removed by exposure of the tubes to a magnet. After being washed, the ab-conjugated beads were incubated with either total cell lysates (200 μg) or subcellular fractions (100 μg) overnight. One-tenth of each lysate was used as the input. After overnight incubation, unbound cell extracts were removed. After 3 washes, elution buffer was added, and the co-precipitated molecules were analyzed in western blot analysis with the appropriate antibodies.

Cytology and immunohistochemistry

Human patient tissues were obtained from the Simmons Cancer Center's Tissue Management Shared Resource. Tumor tissues were fixed in 10% (v/v) formaldehyde in PBS, embedded in paraffin, and cut into 5-μm sections. Tumor tissue sections were deparaffinized in xylene solution, rehydrated, and processed for immunostaining. The antigen retrieval process was performed in 10 mM citric buffer, pH 6.0, for 20 min in a pressure cooker before staining. After staining, the tissues were counterstained with hematoxylin. Abs to the following were used: Par3 (PA5-58475, 1:200, Invitrogen), E-cad (7904497, 1:200, Ventana-Roche, Tucson, AZ), vimentin (347M-18, 1:200, Cell Marque, Rocklin, CA), YAP (sc-101199, 1:200, Santa Cruz), and p-YAP (Ser127, MBS9601097, 1:200, My Biosource). The research was conducted with the approval of the Ethics Committee of University of Texas Southwestern Medical Center on May 10, 2022 (approval No. STU-2022-0162).

Statistical analysis

The data are presented as mean ± SEM. To compare differences between 2 groups with normal data distribution, we used Student's *t*-tests. A P-value ≤ 0.05 was considered statistically significant.

Results

Par3 promotes metastatic behavior of RCC cells

To investigate the role of Par3 in promoting metastatic behavior in RCC cells, we manipulated Par3 levels in 2 metastatic RCC cell lines. Because of the lower endogenous levels of Par3 in Caki-1 cells than ACHN cells (**Figure 1A**), we established Caki-1 Par3 OE cells (expression of metastatic markers in RCC lines in **Figure S1A**). We observed higher expression of several metastatic markers in Par3 OE Caki-1 (Caki-1Par3-2 and Caki-1Par3-4) cells than vector control (Caki-1vec) cells (**Figure 1B**). Functional assays revealed that the Caki-1Par3-2 and Caki-1Par3-4 cells consistently exhibited higher migration/invasion ability than the Caki-1vec cells (**Figure 1C**).

The effect of Par3 on RCC metastasis was further analyzed in a series of ACHN-derived metastatic sublines from brain, bone, lung, and kidney tissue[34,35] (described in **Figure S1B**). We observed higher levels of metastatic markers (**Figure 1D**) and Par3 (**Figure 1E**) in the metastatic sublines than in wt cells. We also performed IHC staining on mouse tumor tissues obtained from metastatic sites, which were the sources of the ACHN sublines. We detected higher Par3 levels in tissues from metastatic sites than in wt tumor tissues obtained from the injection of original ACHN cells (**Figure S1C**), in agreement with the cell line data (**Figure 1E**).

Expression of these metastatic markers in these sublines decreased after Par3 KD with a specific siRNA (**Figure 1F**), thus suggesting the potential effects of Par3 on the metastatic

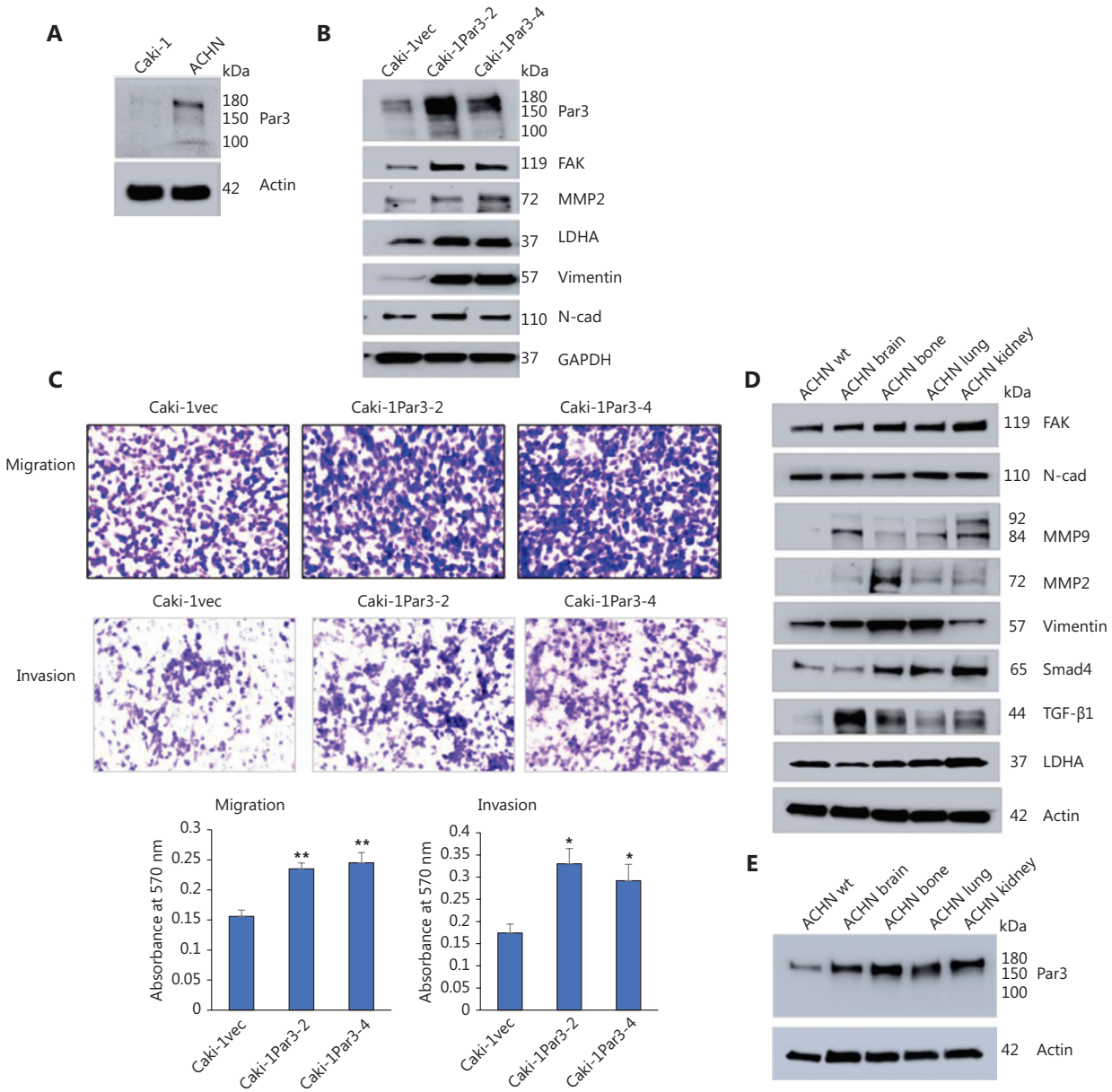


Figure 1 Continued

behavior of these cells. In functional assays, we observed higher migration/invasion ability in 2 metastatic sublines (ACHN bone and ACHN lung) than in wt cells (**Figure 1G**).

Analysis of Par3 levels in RCC patient tissues

To validate the *in vitro* results, we analyzed Par3 levels in patient tissues with RCC of various World Health Organization (WHO) grades. Information regarding these tissues is provided in **Table S2**. Analysis of Par3 expression levels indicated greater Par3 levels in tumor samples than in normal tissues (normal kidney tissues adjacent to tumors) (**Figure 2A**).

Next, an investigation of Par3 levels in tumor tissues of different grades revealed higher Par3 levels (**Figure 2B**) and higher expression of metastatic markers in grade 3 and 4 tissues than in lower grade tissues.

We further analyzed Par3 levels in tissues obtained from distinct sites [non-malignant (normal kidney tissues adjacent to primary tumors), primary tumors, and metastatic sites] in 4

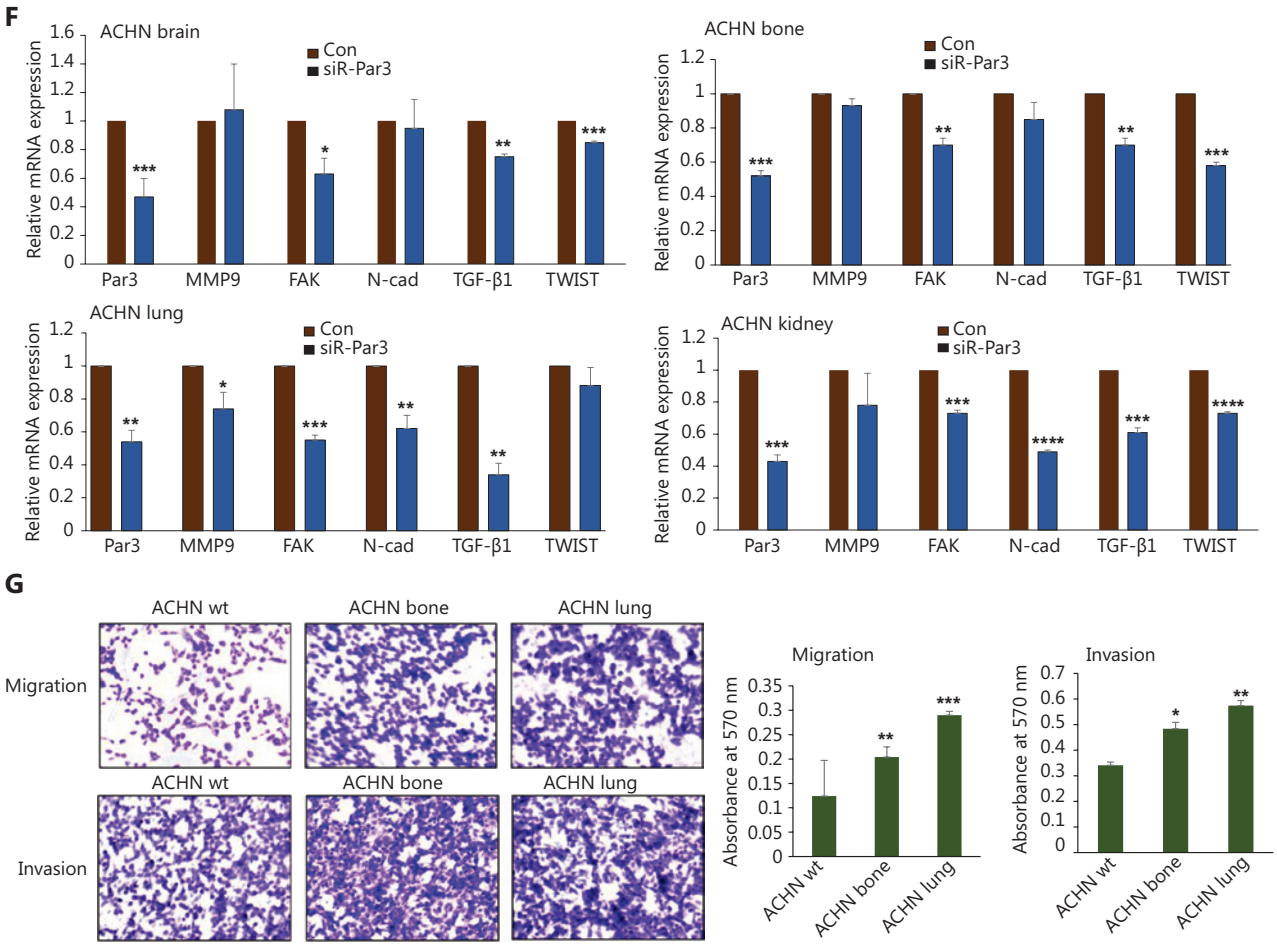


Figure 1 Par3 promotes the metastatic behavior of RCC cells. A. Western blot analysis of Par3 in Caki-1 and ACHN cells. B. Western blot expression of metastatic markers in Par3 overexpressing Caki-1 cell lines (Caki-1vec, Caki-1Par3-2, and Caki-1Par3-4 cells). C. Migration and invasion assays in the Par3 overexpressing Caki-1 cell line. Cells (Caki-1vec, Caki-1Par3-2, and Caki-1Par3-4) were plated in the upper chamber in Transwell plates (8 μm pore size) and assessed at 12 h for migration and at 24 h for invasion experiments. Quantification of three independently performed experiments was performed. D, E. Western blot analysis of (D) metastatic markers and (E) Par3 in ACHN sublines (wt and metastatic sublines). F. qPCR analyses showing transcriptional levels of *PARD3* and metastatic gene markers in Par3 knockdown and sc control ACHN brain, ACHN bone, ACHN lung, and ACHN kidney sublines. G. Metastatic ACHN cell line migration and invasion assays. ACHN wt, ACHN bone, and ACHN lung cells were plated in the upper chamber of Transwell plates (8 μm pore size) and assessed at 12 h for migration and at 24 h for invasion experiments. Quantification of three independent experiments was performed. *P < 0.05, **P < 0.01, ***P < 0.001.

patients (tissue data in **Table S3**). Protein analysis *via* western blotting demonstrated (i) higher Par3 levels in tumors than in normal tissues and (ii) higher Par3 levels in metastatic tumor tissues than primary tumor tissues (**Figure 2C**).

Interestingly, the 100 kDa Par3 isoform was the major detected isoform in metastatic tissue analysis (**Figure 2**), whereas the 180 kDa isoform was the major isoform in metastatic cell studies (**Figure 1**). We analyzed the distribution of 2 isoforms in cell lines and tissues by quantifying data from 3 cell lines and 3 tissue samples. The 180 kDa and 100 kDa isoforms predominated in cell line data and tissue data, respectively (**Figure 2D**).

We then performed IHC staining of tissue sample sets (normal, primary tumors, and metastatic tumor sites) from patients A and B (**Figure 2E**), as well as patient E (**Figure S2**). Staining of epithelial-to-mesenchymal transition markers such as E-cad (an epithelial cell marker, top row of each figure) and vimentin (mesenchymal marker, middle row of each figure) revealed a lower number of E-cad-stained cells, and a higher number of vimentin-stained cells, in the metastatic tissues than

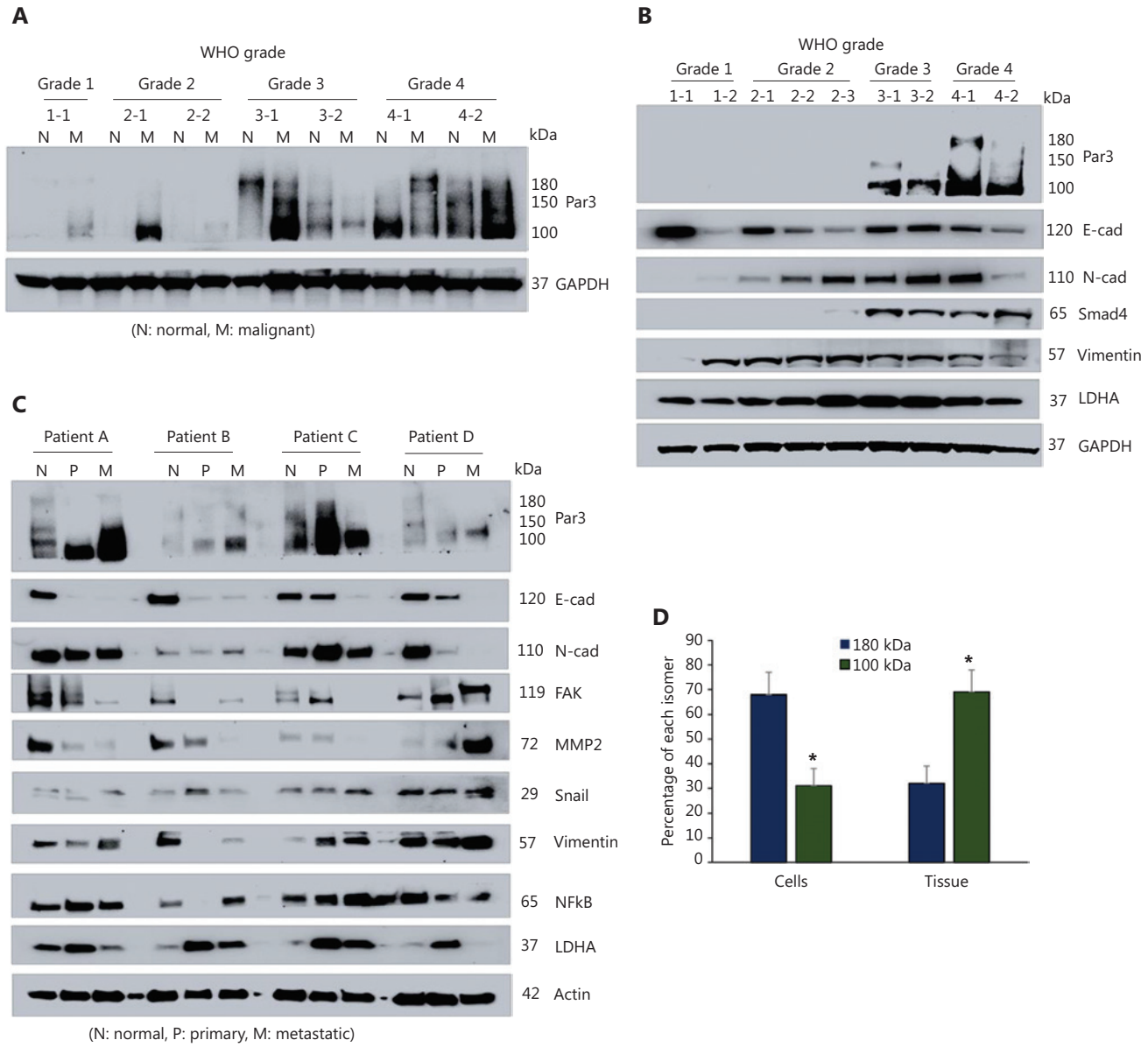


Figure 2 Continued

the matched normal and primary tumor tissues from each patient, as expected. In agreement with the western blot data in **Figure 2C**, we observed higher levels of Par 3 in metastatic tissues than in normal and primary tissue (bottom row of each figure).

Par3 interacts with YAP/TAZ in RCC cells

Par3 has been reported to co-localize with YAP in the nucleus in proliferating canine kidney MDCK cells[28]. To assess whether Par3 might interact with YAP and subsequently modulate YAP/TAZ activity in RCC tumor cells, we examined YAP levels in tumor samples and adjacent normal kidney tissue. Like Par-3 levels, YAP and TAZ levels were also higher in metastatic tumors than in normal tissues and primary tumors, according to IHC (**Figure 3A**) and western blotting (**Figure 3B**).

Moreover, we observed similar expression patterns of Par3 and YAP/TAZ in the ACHN cell line (wt and metastatic sublines) (**Figure 3C**), particularly in the nuclear fractions (**Figure 3D**).

Subsequently, we examined whether Par3 and YAP/TAZ might interact with each other in the nucleus in RCC cells. In

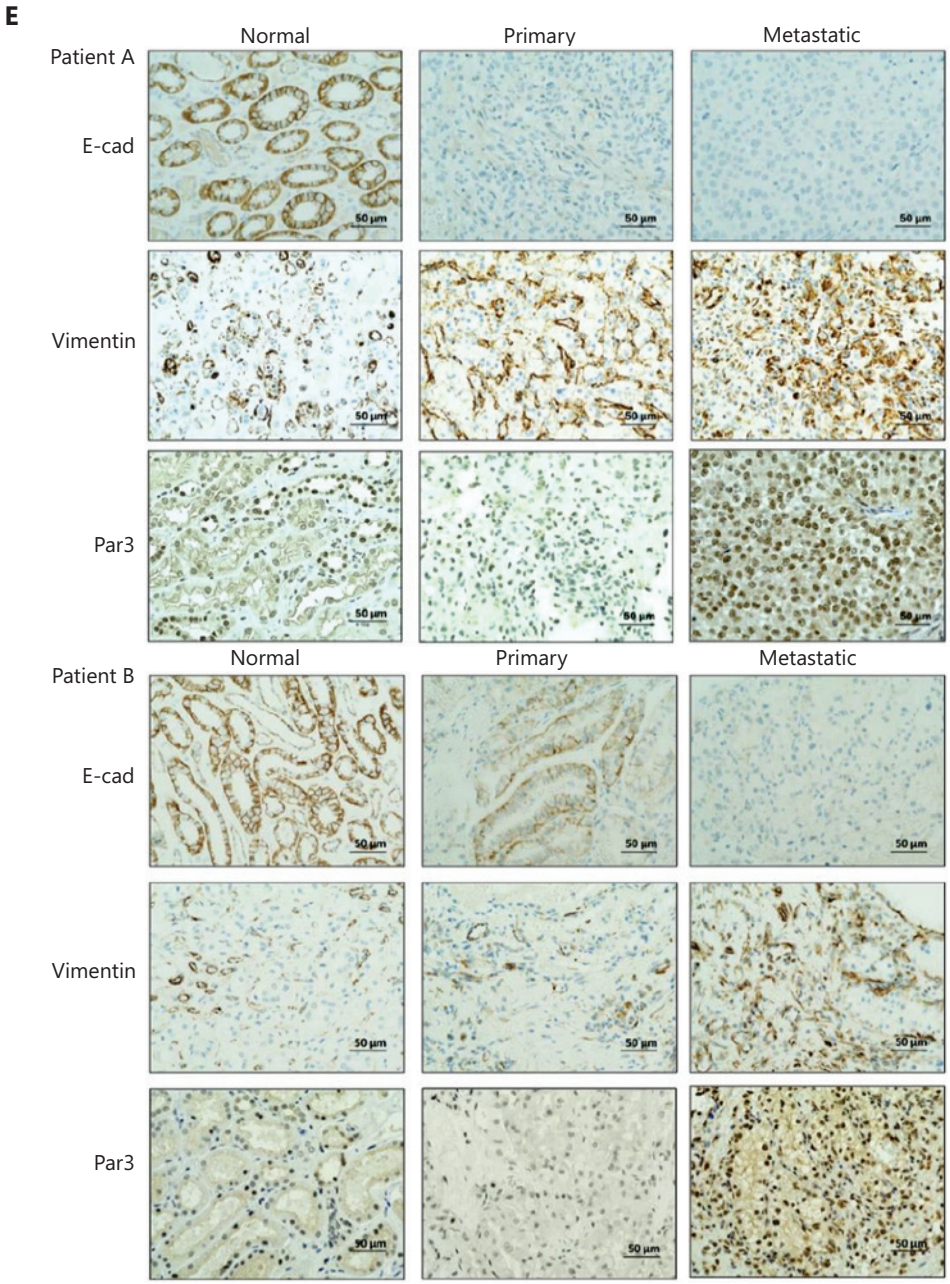


Figure 2 IHC determines Par3 expression in human RCC tissues. A. Western blot analysis of Par3 in non-malignant (normal) and malignant (RCC) patient tissues of various WHO grades. Non-malignant tissues were obtained from kidney tissues adjacent to tumor sites. B. Western blot analysis of Par3 and metastatic marker levels in RCC patient tissues of various WHO grades. C. Western blot analysis of Par3 and metastatic marker levels in tissues of four patients (A–D) obtained from different sites [non-malignant (N), primary (P), and metastatic (M)]. D. Distribution of 2 isoforms in cell line and tissue data. The 180 kDa and 100 kDa band intensities from three cell line data sets shown in **Figure 1A, 1B**, and **1C** and three tissue datasets shown in **Figure 2A** and **2B** were quantified with ImageJ. E. IHC staining of vimentin, E-cad, and Par3 in tumor tissues of patients A and B. Magnification, 40×. *P < 0.05.

nuclear fractions of Caki-1vec, Caki-1Par3-2, and Caki-1Par3-4 cells, using abs to Par3, we detected co-immunoprecipitated YAP and TAZ proteins (**Figure 3E**, left). Similarly, using abs to YAP, we detected co-immunoprecipitated TAZ and Par3 proteins (**Figure 3E**, middle). Input analysis data are shown in the right panel in **Figure 3E**.

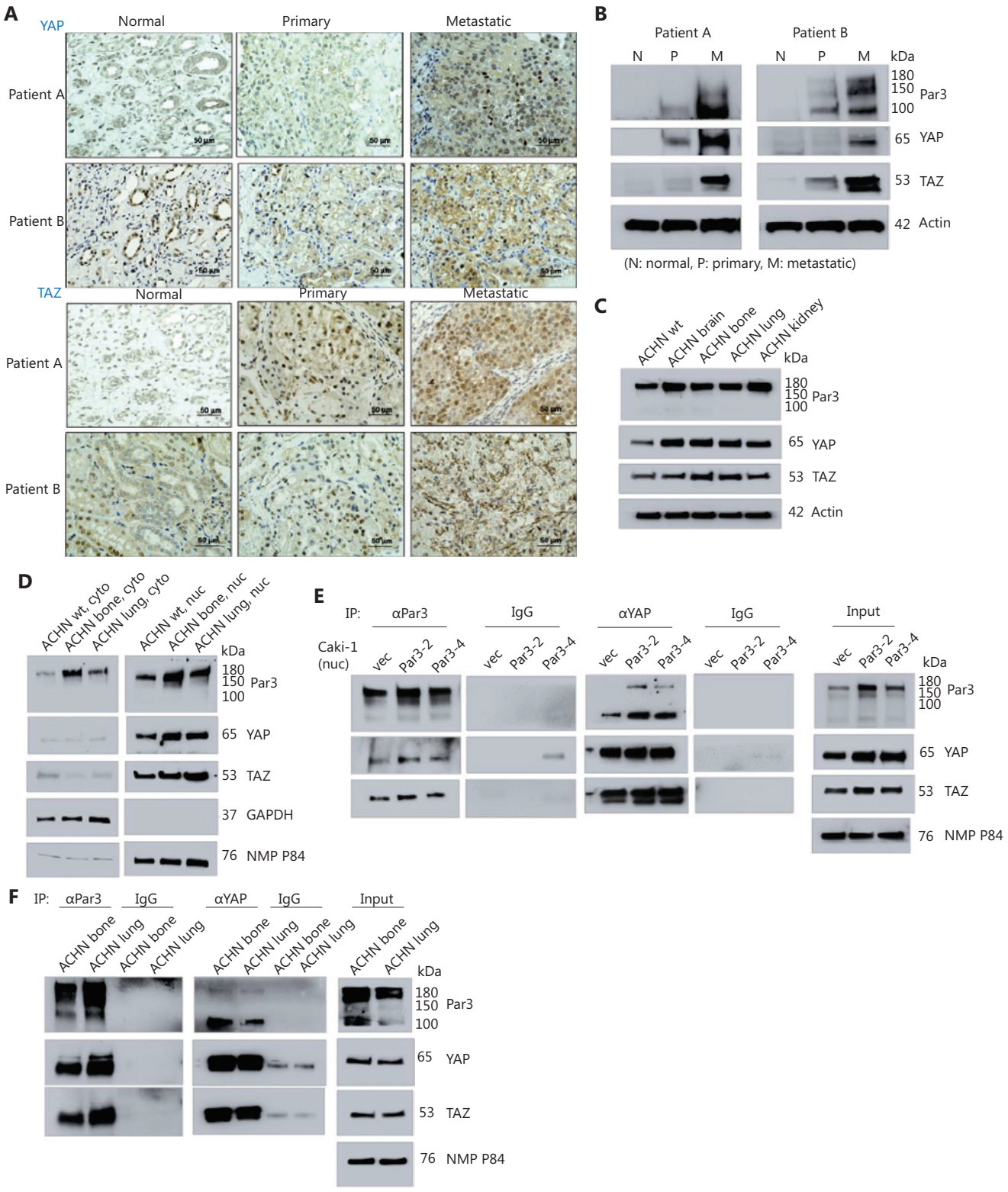


Figure 3 Continued

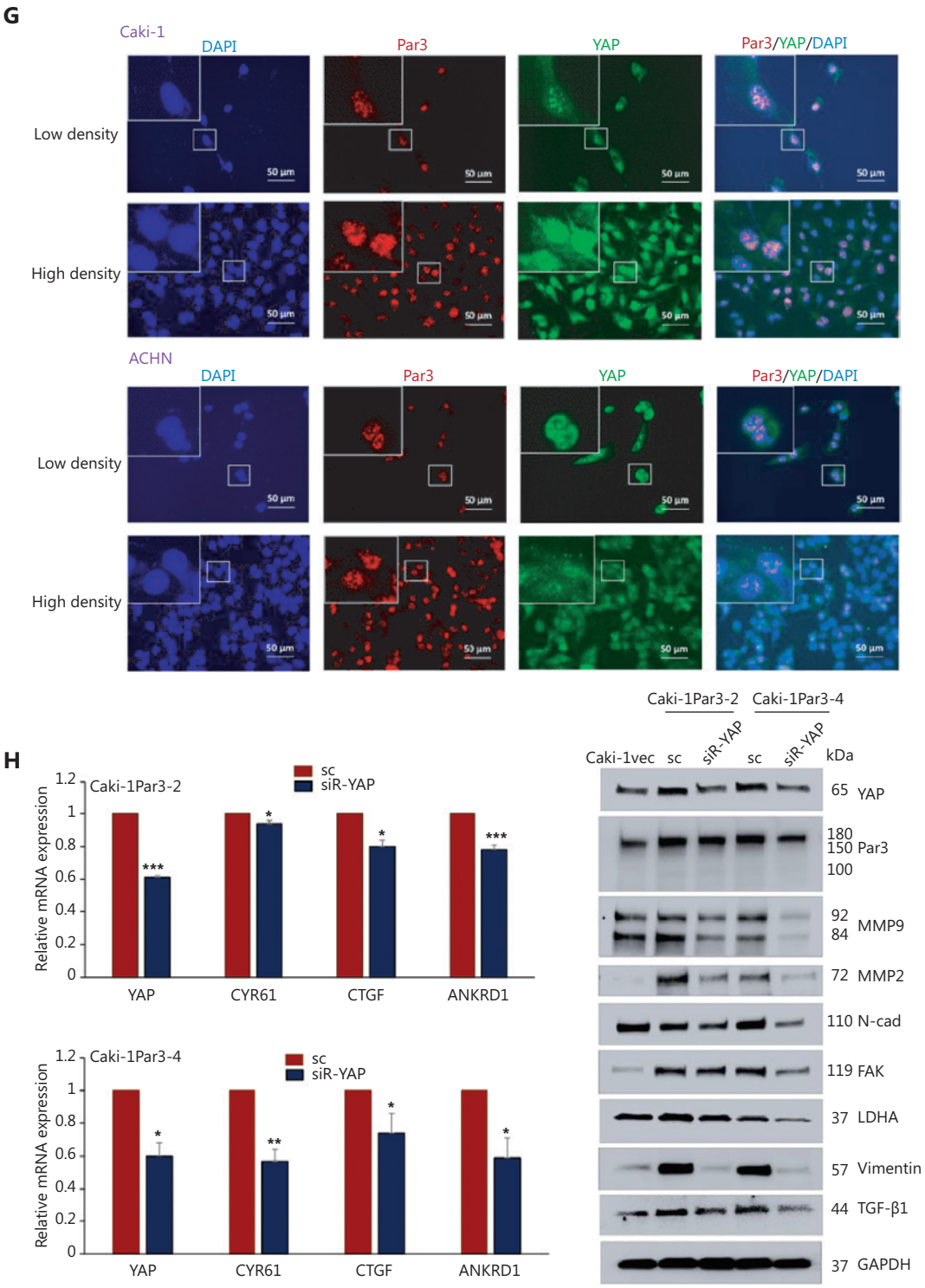


Figure 3 Par3 interacts with YAP/TAZ in RCC cells. A, B. YAP/TAZ IHC staining in RCC tissue obtained from various sites (non-malignant, primary, and metastatic) in patients A and B. Magnification, 40×. C. Western blot analyses of Par3, YAP, and TAZ levels in the ACHN cell set (wt and metastatic organ-derived cell lines). D. Western blot analysis of Par3 and YAP in the cytoplasmic and nuclear fractions of ACHN wt, ACHN bone, and ACHN lung cells. GAPDH and nuclear matrix protein P84 (NMP P84) were used as internal controls of cytoplasmic and nuclear fractions, respectively. E, F. Co-immunoprecipitation study results. Nuclear extracts (100–200 μg) of (E) Caki-1vec, Caki-1Par3-2, and Caki-1Par3-4

cells and (F) ACHN bone and ACHN lung cells were immunoprecipitated with abs to either Par3 or YAP, and co-immunoprecipitated proteins were analyzed with western blotting. The input (1/10th of nuclear extracts used in the co-IP experiment) analysis result is shown at the right in each figure. G. Immunofluorescence (IF) staining results. Caki-1 and ACHN cells at two cell densities were stained with abs to Par3 and YAP, followed by anti-rabbit Cy5 (red) and anti-mouse Alexa488 (green) secondary abs. Magnification, 40× (inserts, 60×). H. Western blot analysis of metastatic marker levels in Caki-1Par3-2 and Caki-1Par3-4 cells after transfection with either siR-YAP or sc control plasmids (right). The left panel shows qPCR analysis results demonstrating decreased expression of YAP downstream genes after siRNA-mediated YAP KD. *P < 0.05, **P < 0.01, ***P < 0.001.

Similar co-IP experiments on nuclear fractions from the ACHN bone and ACHN lung sublines (**Figure 3F**), as well as from parental Caki-1 and ACHN cells (**Figure S3**), also demonstrated interaction between Par3 and YAP/TAZ proteins.

We further investigated the co-localization of Par3 and YAP *via* IF staining. Co-localization of these 2 proteins was detected in the nucleus in Caki-1 cells (**Figure 3G**, upper) and ACHN (**Figure 3G**, lower) cells at 2 different cell densities, thus also supporting the hypothesis that Par3 interacts with YAP in the nucleus in RCC cells.

To further confirm the interaction of Par3 and YAP molecules, we assessed the effects of YAP KD on the expression of metastatic markers in Caki-1Par3-2, Caki-1Par3-4, and Caki-1vec cells. qPCR data (**Figure 3H**, left) demonstrated diminished transcription of the YAP-regulated genes *CYR61*, *CTGF*, and *ANKRD1* in siRNA-YAP transfected Caki-1Par3-2 and Caki-1Par3-4 cells, thus indicating the specificity and effectiveness of siRNA-YAP. Under these conditions, KD of YAP in these cells reversed the elevated expression of metastatic markers associated with Par3 OE (**Figure 3H**, right).

Par3 promotes YAP/TAZ transcriptional activity

Given the interaction between Par3 with YAP/TAZ, we subsequently investigated the effect of this interaction on downstream gene transcription by YAP/TAZ. First, we analyzed the transcriptional levels of the YAP/TAZ downstream genes *CYR61*, *CTGF*, and *AREG* in Caki-1vec, Caki-1Par3-2, and Caki-1Par3-4 cells. Transcription of these genes was greater in Par3 OE cell lines (Caki-1Par3-2 and Caki-1Par3-4 cells) than vector control (Caki-1vec) cells (**Figure 4A**). In contrast, transcription of the YAP/TAZ downstream genes (*CYR61*, *CTGF*, *ANKRD1*, and *AREG*) was lower in Par3 KD (siR-Par3) ACHN bone (**Figure 4B**, left) and ACHN lung (**Figure 4B**, right) cells than in sc control cells. These results were confirmed through western blot analysis. As shown in **Figure 4C** (Caki-1vec/Caki-1Par3-2/Caki-1Par3-4 cell set data) and **Figure 4D** (ACHN bone sc/siR-Par3 and ACHN lung sc/siR-Par3 cell set data), Par3 regulated the expression of YAP downstream molecules.

We next measured the luciferase activity of the YAP/TAZ reporter (8xGTIIC-lux) in RCC cells after manipulation of Par3 levels. Higher Par3 levels correlated with greater luciferase activity in cell lines with stable Par3 OE (Caki-1Par3-2 and Caki-1Par3-4 cells) than in vector control (Caki-1vec) cells (**Figure 4E**). Elevated luciferase activity was also detected in Caki-1 (**Figure 4F**), ACHN (**Figure 4G**), and HEK293 (**Figure 4H**) cells after transient transfection of the Par3 expression vector. Moreover, Par3 KD resulted in lower luciferase activity in ACHN (**Figure 4I**), ACHN bone (**Figure 4J**), and ACHN lung (**Figure 4K**) cells than observed in sc control cells.

The PDZ domain 3 of PARD3 is critical for its interaction with YAP/TAZ and subsequent YAP/TAZ transcriptional activation

The Par3 protein contains 3 PDZ domains, whereas both YAZ and TAZ proteins have one PDZ binding domain each[37,38] (**Figure 5A**). To further investigate which PDZ domain of *PARD3* is critical for interaction with YAP/TAZ molecules, we used several Par3 mutants with domain deletions of PDZ1, 2, 3, or 1/3 (denoted Δ1-Par3, Δ2-Par3, Δ3-Par3, and Δ1/3-Par3), as previously described[36]. Caki-1 cells were transfected with either FL-Par3 or domain-deleted mutant forms of Par3, and immunoprecipitation with either YAP ab or Par3 ab was performed. We observed less interaction of Par3-YAP/TAZ in cells transfected with Δ3-Par3 and Δ1/3-Par3 than with other constructs (**Figure 5B**). These findings indicated that Par3 interacted less with YAP when PDZ3-deletion mutants were introduced, because these mutants diminished YAP interaction.

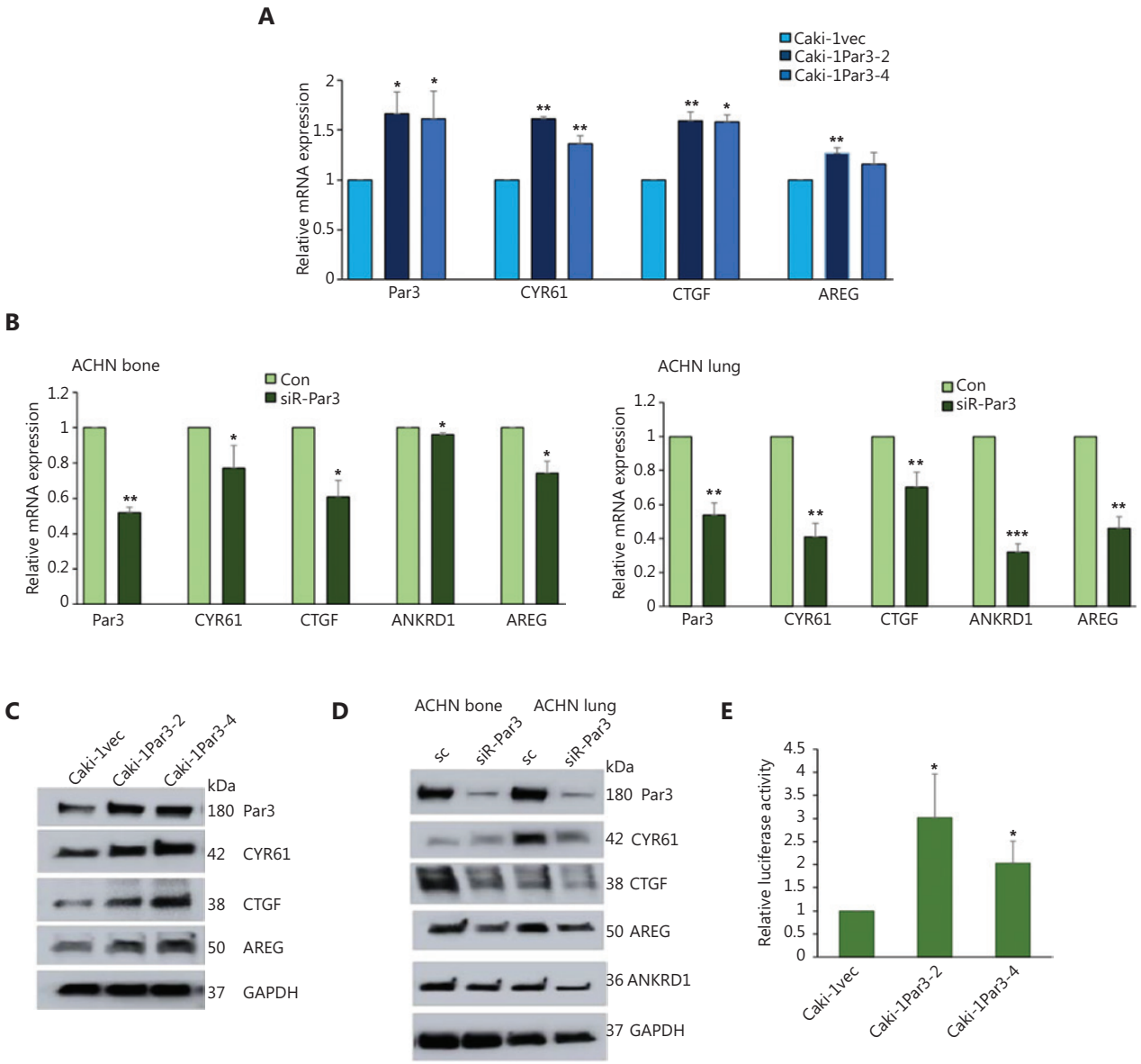


Figure 4 Continued

A similar experiment in HEK293T cells also confirmed the diminished Par3-YAP/TAZ interaction in cells transfected with Δ3-Par3 (**Figure S4A**). These results suggested that PDZ domain 3 is critical for the interaction between Par3 and YAP/TAZ. Consistently, we observed lower transcription of the YAP/TAZ downstream genes *CYR61* and *CTGF* (**Figure 5C**), and lower YAP/TAZ reporter luciferase activity, in Caki-1 (**Figure 5D**) or HEK293T (**Figure S4B**) cells transfected with Δ3-Par3 or Δ1/3-Par3 vectors rather than other constructs. Western blotting also demonstrated lower expression of metastasis markers in Caki-1 cells transfected with Δ3-Par3 or Δ1/3-Par3 plasmids than observed in cells transfected with other constructs (**Figure 5E**).

Par3 enhances YAP/TAZ levels and promotes nuclear translocation of YAP

We next investigated whether Par3 might control intracellular levels of YAP/TAZ in RCC cells. We detected greater YAP and TAZ protein levels in Par3 overexpressing Caki-1Par3-2

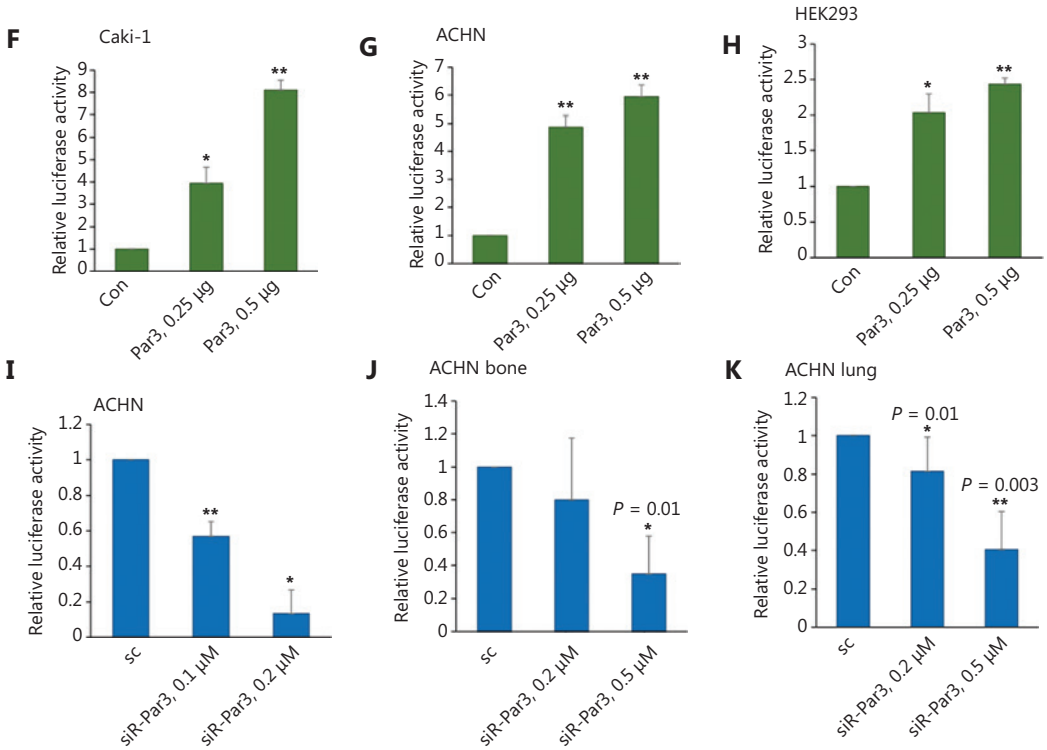


Figure 4 Par3 promotes YAP/TAZ activity. A. qPCR analyses analyzing transcriptional levels of the *PARD3* and YAP/TAZ downstream genes *CYR61*, *CTGF*, and *AREG* in Caki-1vec, Caki-1Par3-2, and Caki-1Par3-4 cells. B. qPCR analyses of the transcriptional levels of the *PARD3* and YAP/TAZ downstream genes *CYR61*, *CTGF*, *ANKRD1*, and *AREG* in Par3-knockdown ACHN bone (left) and ACHN lung (right) cells and the respective sc control cells. C, D. Western blot analysis of YAP downstream molecules in (C) Caki-1vec, Caki-1Par3-2, and Caki-1Par3-4 cells and (D) in ACHN bone sc/siR-Par3 and ACHN lung sc/siR-Par3. E–H. Luciferase assay results with Par3 level manipulation. YAP/TAZ reporter activity was measured in (E) Caki-1vec/Caki-1Par3-2/Caki-1Par3-4 cells, (F) Caki-1 cells with co-transfection of Par3 expression vector, (G) ACHN cells with co-transfection of Par3 expression vector, and (H) HEK293T cells with co-transfection of Par3 expression vector. I–K. Luciferase assay results in cells with Par3 KD. YAP/TAZ reporter activity was measured in (I) ACHN cells, (J) ACHN bone cells, and (K) ACHN lung cells after co-transfection with siPar3 RNA constructs. **P* < 0.05, ***P* < 0.01, ****P* < 0.001.

and Caki-1Par3-4 cells than in Caki-1vec cells (**Figure 6A**, left, western blot data; right, qPCR data). Meanwhile, we observed downregulation of YAP and TAZ molecules in Par3 KD ACHN bone (**Figure 6C**, left) and ACHN lung (**Figure 6C**, right) cells than in sc control cells. These results suggested that Par3 upregulates YAP/TAZ levels, as further evidenced by greater IHC staining of Par3 (**Figure 2E**) and YAP (**Figure 3A**) in metastatic patient tissues than in normal and primary tissues. In contrast to YAP, we detected lower phosphorylated YAP (p-YAP) levels in metastatic tissues than in normal and primary tissues (**Figure 6D**; quantification of positively stained cells shown at right).

Notably, the positive staining was concentrated in the nuclear region in normal tissues but was observed in the cytoplasm in primary and metastatic tissues. Given the significantly differing YAP and p-YAP levels, we examined whether Par3 might modulate YAP/TAZ (nuclear) and p-YAP (cytoplasmic) levels in RCC cells. We first analyzed YAP and p-YAP levels in the cytoplasmic and nuclear fractions of Caki-1vec, Caki-1Par3-2, and Caki-1Par3-4 cells. Nuclear YAP levels were higher, whereas cytoplasmic p-YAP levels were lower, in Caki-1Par3-2 and Caki-1Par3-4 cells than in Caki-1vec cells (**Figure 6E**). In contrast, we detected lower nuclear YAP levels, and higher cytoplasmic p-YAP levels, in Par3 KD ACHN lung and ACHN bone cells than in sc control cells (**Figure 6F**).

Par3 regulation of YAP nuclear transport was further supported by IF staining results. We used 2 sets of cells: (i) the

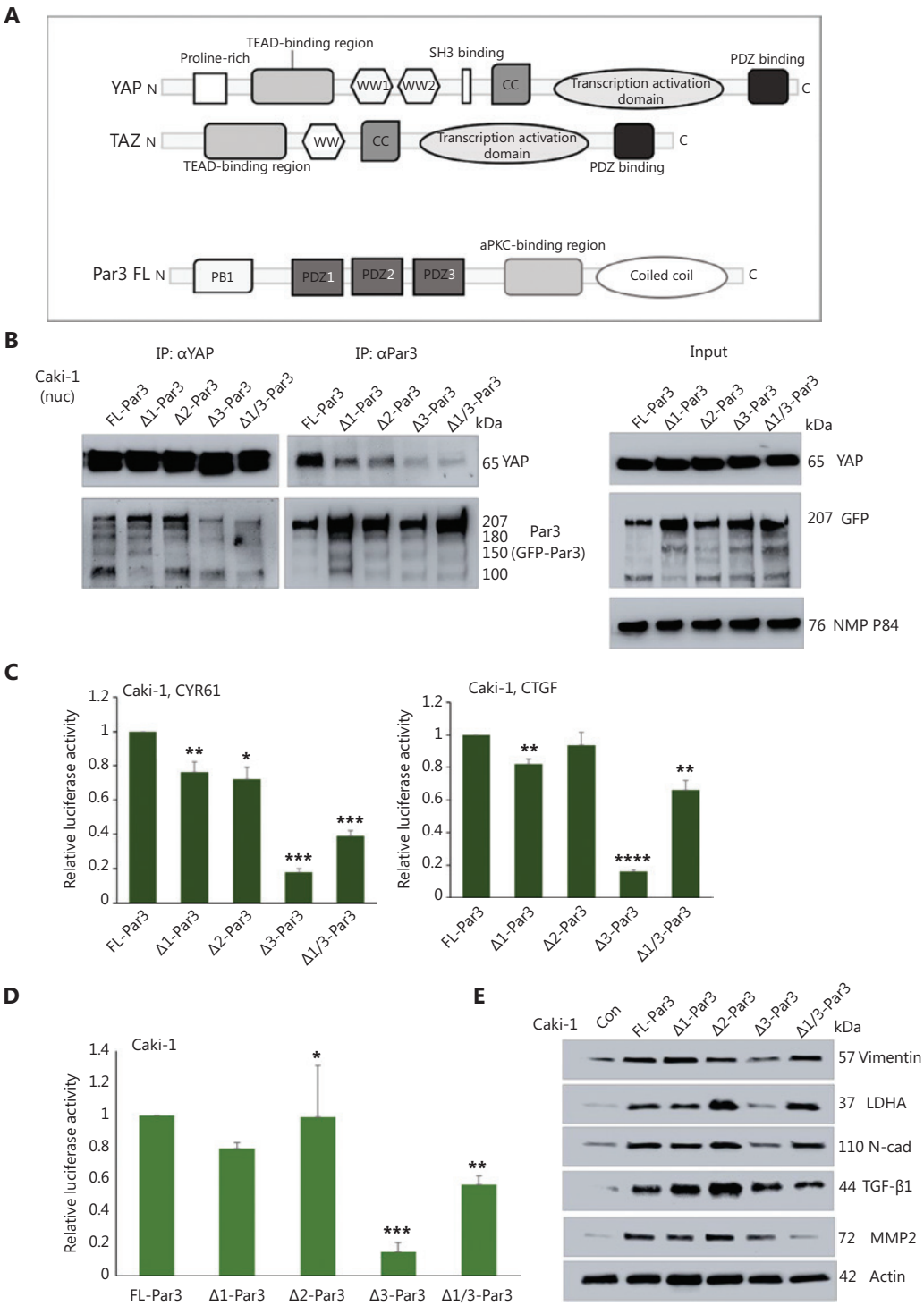


Figure 5 PDZ domain 3 of Par3 is essential for YAP/TAZ interaction. A. Diagram of the domain architecture of *YAP*, *TAZ*, and *PARD3* genes. B. Assessment of YAP and Par3 interaction by co-immunoprecipitation with Par3 deletion constructs in Caki-1 cells. Caki-1 cells were transfected with FL-Par3, PDZ domain 1 deletion mutant (Δ1-Par3), PDZ domain 2 deletion mutant (Δ2-Par3), PDZ domain 3 deletion mutant (Δ3-Par3), or PDZ domain 1 and 3 double deletion mutant (Δ1/3-Par3), and immunoprecipitated with either YAP ab or Par3 ab. C. qPCR analysis of the YAP downstream genes *CYR61* and *CTGF* in Par3 construct-transfected cells. D. Luciferase activity was assessed after 24 h in Caki-1 cells after co-transfection with Par3 constructs and YAP/TAZ reporter (8xGTIIC-lux). E. Western blot analysis of metastatic markers after transfection of Par3 deletion constructs in Caki-1 cells. *P < 0.05, **P < 0.01, ***P < 0.001, ****P < 0.0001.

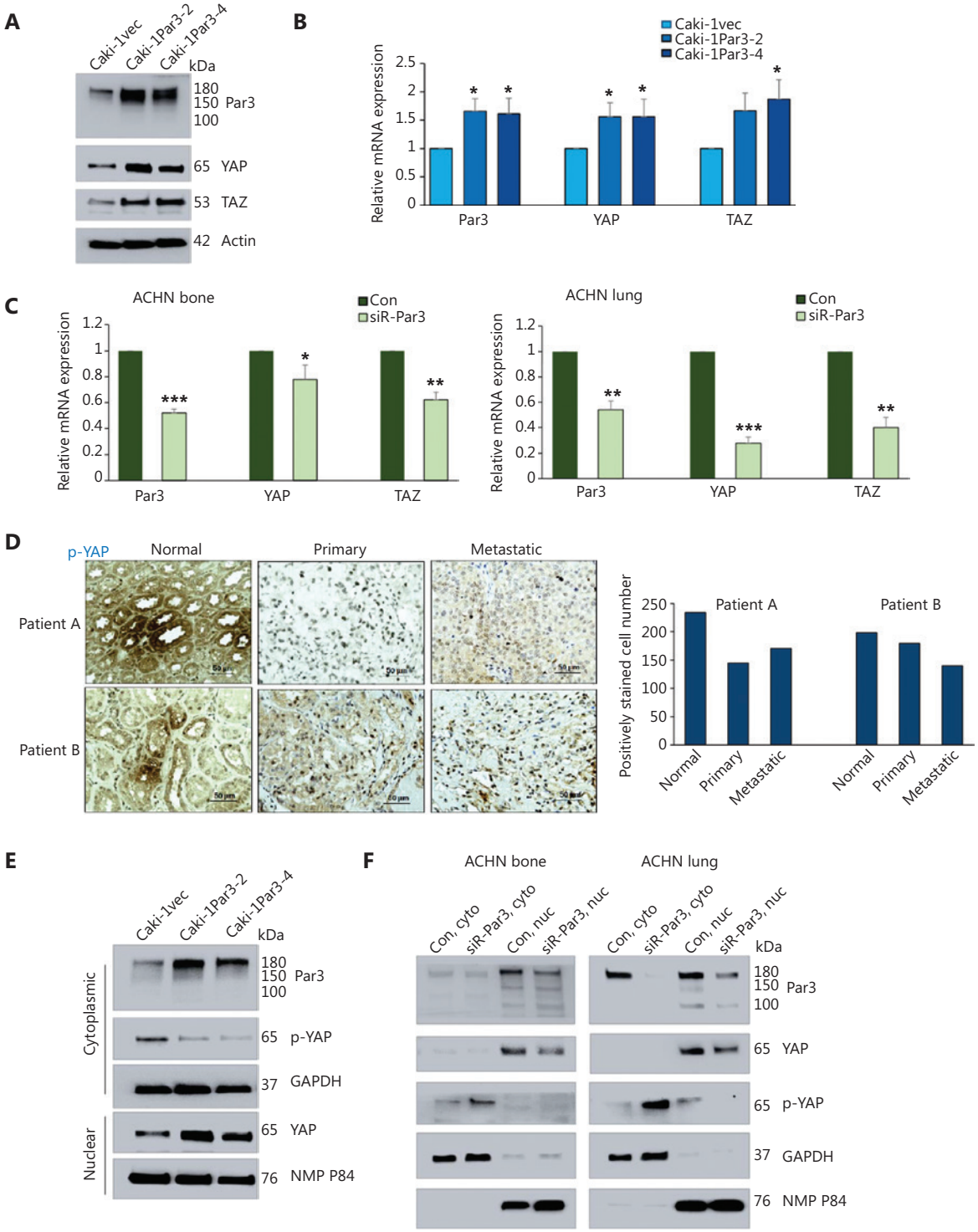


Figure 6 Continued

Caki-1vec/Caki-1Par3-2/Caki-1Par3-4 cell set and (ii) the ACHN bone sc/siR-Par3 and the ACHN lung sc/siR-Par3 cell set. We subsequently examined YAP distribution in the cytoplasmic and nuclear fractions. Higher amounts of YAP were present in the nuclear fraction of Caki-1Par3-2 and Caki-1Par3-4 cells than Caki-1vec cells (**Figure 6G**). Moreover, the

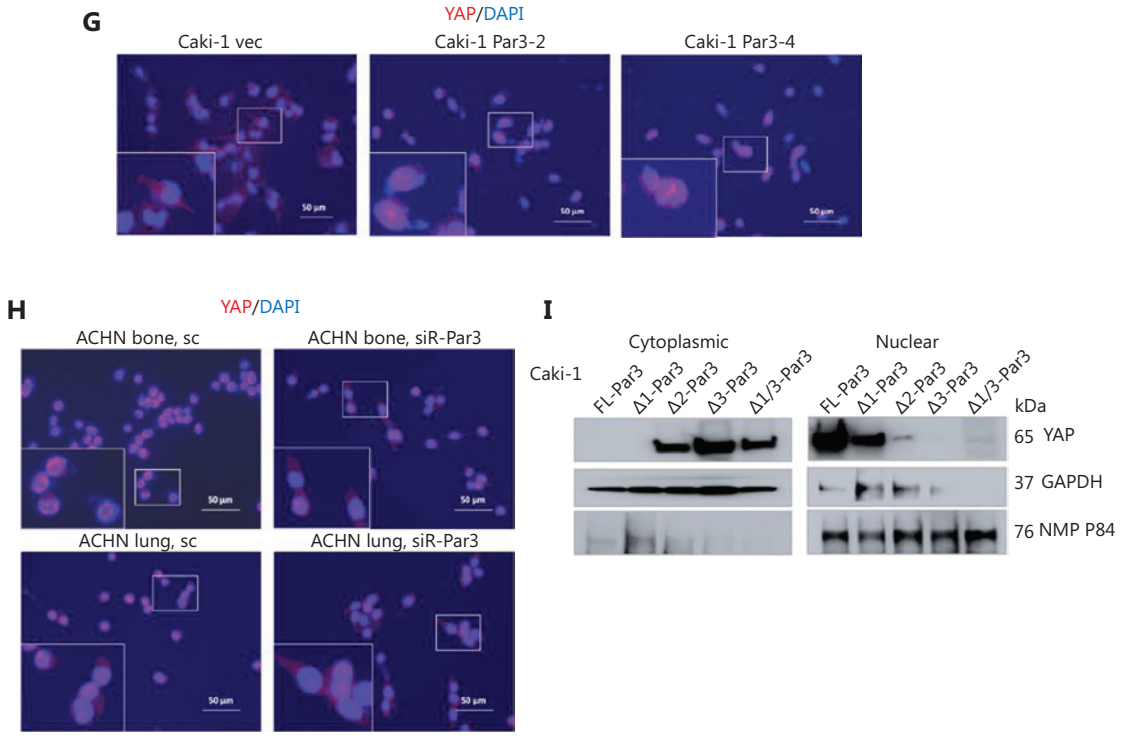


Figure 6 Par3 upregulates YAP/TAZ levels and promotes nuclear translocation of YAP. A. Western blot of Par3 and YAP levels in Caki-1vec, Caki-1Par3-2, and Caki-1Par3-4 cells. B. qPCR analysis of *YAP1* and *TAZ* genes in Caki-1vec, Caki-1Par3-2, and Caki-1Par3-4 cells. C. qPCR analysis of *PARD3*, *YAP1*, and *TAZ* genes in ACHN bone (left) and ACHN lung (right) cells. D. IHC staining of p-YAP in tissue sets from patients A and B. Magnification, 40×. Quantification of positively stained cells is shown at right. Counting of positively stained cells was performed in ImageJ software. E. Western blot of cytoplasmic p-YAP and nuclear YAP levels in Caki-1vec, Caki-1Par3-2, and Caki-1Par3-4 cells. F. Western blot of cytoplasmic p-YAP and nuclear YAP levels in Par3 KD ACHN bone (left) and ACHN lung (right) cells, and sc control cells. G, H. YAP IF staining in (G) Caki-1vec, Caki-1Par3-2, and Caki-1Par3-4 cells and (H) in ACHN bone sc/siR-Par3 (upper) and ACHN lung sc/siR-Par3 (lower). Magnification, 40× (insets, 60×). I. Western blot analysis of YAP in the cytoplasmic and nuclear fractions of Par3 mutant-transfected cells. $^{*}P < 0.05$, $^{**}P < 0.01$, $^{***}P < 0.001$.

YAP distribution in the nuclear fraction decreased after Par3 KD (**Figure 6H**, ACHN bone cell data, top; ACHN lung cell data, bottom), thus supporting that Par3 promotes nuclear translocation of YAP.

To demonstrate the critical role of the Par3 domain in mediating YAP nuclear transport, we analyzed YAP levels in the cytoplasmic and nuclear fractions of Par3 mutant-transfected cells. As shown in **Figure 6I**, nuclear YAP levels were diminished and cytoplasmic YAP levels were elevated in Δ2-Par3, Δ3-Par3, and Δ1/3-Par3-transfected Caki-1 cells. These effects were most pronounced in cells transfected with Δ3-Par3. This finding suggested that domain 3 not only is important in the binding of Par3 with YAP but also is critical in mediating nuclear transport of YAP.

Discussion

Herein, we first sought to determine whether Par3 plays a negative or positive role in RCC metastasis, given that published data support differing roles of Par3 according to cancer type[9,11,18-23]. Using 2 metastatic RCC models (Caki-1 and ACHN cell lines) (**Figure 1**) and clinical samples (**Figure 2**), we demonstrated the role of Par3 in promoting RCC metastasis. This observation was consistent with prior data indicating an association between Par3 OE and poor prognosis in patients with RCC[23]. However, no studies to date have demonstrated the underlying molecular mechanism of Par3 in RCC progression.

Three Par3 isoforms (180 kDa, 150 kDa, and 100 kDa forms) arise from alternative splicing of the *PARD3* gene[5].

The predominant Par3 isoforms differ among cancer types. For instance, esophageal squamous cell carcinoma appears to express all 3 isoforms in similar proportions[39], whereas the 180 kDa form appears to be the major isoform in bladder cancer[21] and glioma[40]. Meanwhile, the 150 kDa isoform is the major isoform in breast cancer cells[41]. In this study, the Par3 isoform profiles notably differed between RCC cell lines and patient tissues. The 180 kDa isoform was the predominant form of Par3 in most cell lines, whereas the 100 kDa form was the major isoform in tumor tissues. Because the RCC cell lines used in this study were not directly derived from these specific patients with RCC, underlying variations in genetic or histological classifications might explain this difference.

We focused on the downstream effects of elevated Par3 levels on cancer progression and metastasis in RCC. We examined the role of Par3 in regulating YAP activity in the nucleus. Zhou et al.[9] had previously examined the role of Par3 in regulating the Hippo pathway and consequently influencing prostate cancer metastasis. However, they focused on cytoplasmic Par3's role in forming a complex with KIBRA but did not study its direct interaction with YAP/TAZ in the nucleus. Similarly to the findings for YAP, we observed substantial Par3 localization in the nuclei in proliferating cells (**Figure S5**). The

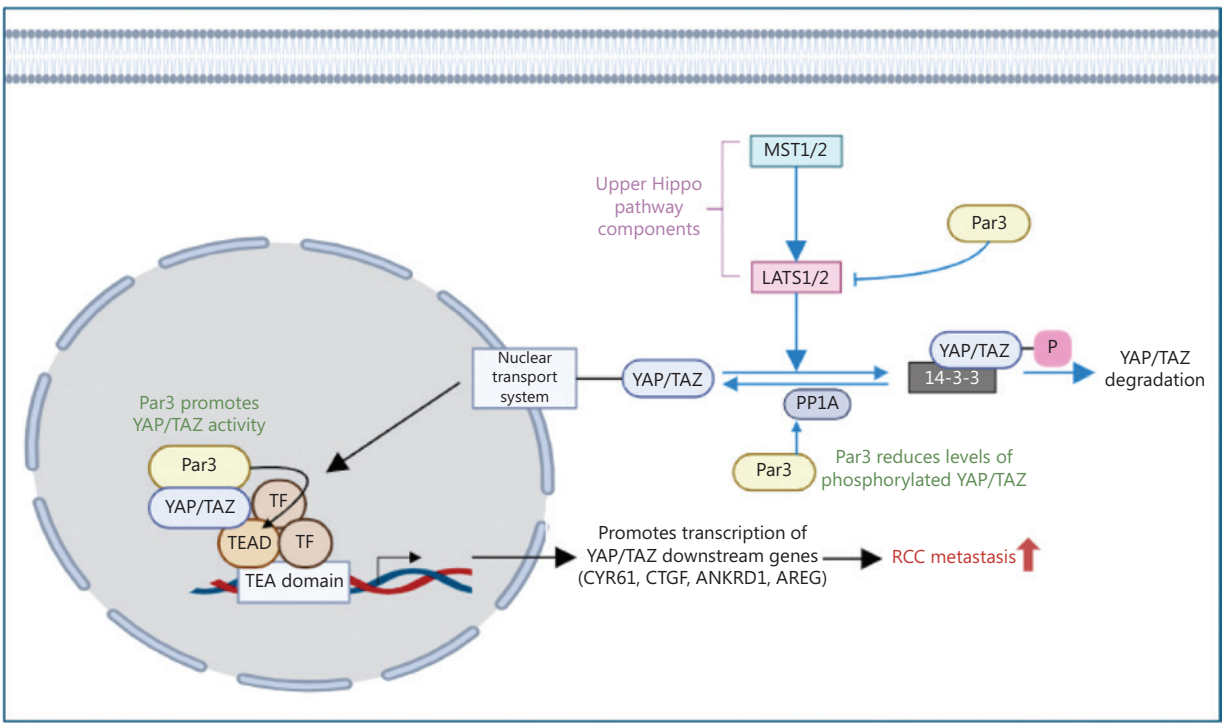


Figure 7 Integrated schematic of Par3 function in YAP/TAZ nuclear translocation and gene transactivation in RCC cell metastasis. Beyond its roles in controlling cell polarity and division, Par3 might also contribute to cancer cell metastasis by regulating YAP/TAZ function in the Hippo pathway. (1) Promotion of YAP/TAZ nuclear translocation *via* regulation of phosphorylation and dephosphorylation: (i) Par3 inhibits the LAST1/2 kinases in the upper Hippo pathway, thus preventing YAP/TAZ phosphorylation[28]. (ii) Protein phosphatase 1 (PP1A) has been reported to bind Par3 and regulate Par3 phosphorylation[7], thereby promoting YAP/TAZ dephosphorylation. Both pathways might promote YAP/TAZ nuclear translocation by preventing cytoplasmic retention and degradation, a process potentially mediated through the interaction of 14-3-3 with the phosphorylated form of YAP[44]. (2) Promotion of YAP/TAZ-mediated transactivation, as shown in this study: Par3 binds YAP/TAZ in a PDZ domain 3-dependent manner in the nucleus and may enhance the transcription of metastasis-relevant candidate genes such as *CYR61*, *CTGF*, *ANKRD1*, and *AREG*, possibly by acting in a complex with TEAD and other TFs. Elevated expression of these genes is associated with increased cancer metastasis[45-48]. Nevertheless, the detailed molecular mechanism underlying such transactivation remains to be explored. Par3, partition defective protein 3; YAP, yes-associated protein; TAZ, transcriptional coactivator with PDZ-binding motif; TF, transcription factor; TEAD, transcriptional enhancer-associated domain; MST1/2, mammalian sterile 20-like kinases 1 and 2; LAST1/2, large tumor suppressor homolog kinases 1 and 2; PP1A, protein phosphatase 1A. Figure created with BioRender (Toronto, Ontario). The lines in blue represent existing findings in the literature.

expression profiles of Par3 and YAP in the nuclear fraction of RCC cells were correlated, thus prompting further investigation into their relationship.

YAP/TAZ are co-transcription factors that mediate cancer progression and metastasis through interaction with TEAD[27,33,42]. Nuclear translocation of YAP is a critical driver of proliferation and metastasis of tumor cells[31]. We confirmed the interaction of Par3 and YAP proteins through co-IP experiments, and demonstrated the co-localization of Par3 and YAP in RCC cell lines (**Figure 3**). Furthermore, interaction with Par3 increased the transcription of YAP/TAZ-regulated genes and enhanced YAP/TAZ transcriptional activity, as evidenced by increased luciferase reporter activity (**Figure 4**). We did not observe an additive or synergistic effect on the transcription of YAP downstream genes (**Figure S6**); therefore, Par3 might act as a cofactor of YAP activation rather than as an independent co-transcription factor. A crucial next step will be investigating the interaction of these 2 proteins at the chromatin level.

We found that the PDZ domain 3 of the Par3 protein is particularly important in Par3-YAP interactions in RCC tumor cells (**Figure 5**). This result aligns with findings from Zhang et al.[28], who have reported an interaction between Par3's PDZ domain 3 and YAP in MDCK cells. We further demonstrated that the attenuated Par3-YAP interaction in a Par3 PDZ domain 3 deletion mutant diminished the transcription of YAP/TAZ-regulated genes (**Figure 5C**), YAP/TAZ transcriptional reporter activity (**Figure 5D**), and metastatic marker levels (**Figure 5E**). Interestingly, the marker levels in Δ1/3-Par3 transfected cells were higher than those observed in Δ3-Par3 transfected cells. We also observed similar results in the luciferase assays and transcription experiments (**Figure 5C and 5D**). We interpreted these findings as suggesting that the additional deletion of the Δ1 domain induces a conformational change that subsequently affects downstream gene and protein expression.

We also demonstrated that Par3 upregulated intracellular levels of YAP and TAZ, and promoted dephosphorylation of YAP at Ser127 as well as its nuclear translocation in RCC cells (**Figure 6**). These findings are consistent with those from Zhang et al.[28], who have shown a similar effect of Par3 on YAP dephosphorylation and its nuclear translocation in normal kidney MDCK cells. Whereas cancer cells were used in other studies, their research focused on the role of cytoplasmic Par3 in controlling the YAP phosphorylation process. Additionally, the role of Par3 in triggering YAP phosphorylation in RCC cells had not been reported previously. Herein, we provide new evidence that the Par3 PDZ domain 3 is important in nuclear transport of YAP. In addition, Lv et al.[43] have shown that Par3 inhibits phosphorylation of TAZ. Whether Par3 mediates the nuclear transport of TAZ warrants future investigation.

In summary, we report that Par3 plays an important role in promoting metastatic potential in RCC. We specifically revealed that the mechanism of Par3 involves (i) physically interacting with the YAP/TAZ protein, functioning as a co-factor of YAP/TAZ activation, (ii) modulating intracellular translocation of YAP to the nucleus, and (iii) upregulating the transcription of YAP/TAZ downstream genes (summary in **Figure 7**).

Notably, elevated levels of Par3 are pro-metastatic in some cancers, whereas in other cancers, diminished Par3 levels are associated with metastasis. Evidence across multiple studies and cancer types has demonstrated that Par3's role in metastasis is indeed cancer specific. Although the exact reasons for this remain unclear, we speculate that, given Par3's central role in multiple critical pathways, both OE and depletion of Par3 might result in adverse effects.

Thus, Par3 appears to have distinct roles, either negative or positive, in metastasis through differing underlying molecular mechanisms.

Conclusions

Par3 plays an important role in promoting metastatic potential in RCC. We specifically revealed that the mechanism of Par3 involves (i) physically interacting with the YAP/TAZ protein, functioning as a co-factor of YAP/TAZ activation, (ii) modulating intracellular translocation of YAP to the nucleus, and (iii) upregulating the transcription of YAP/TAZ downstream genes (**Figure 7**). Future studies should include mouse studies with Par3 OE cells, Par3 KD cells, or patient-derived xenograft mouse models to further clarify the role of Par3 in RCC metastasis.

Grant support

This work was supported by grants from the American Urology Association (AUA) Urology Care Foundation Research Scholar Award, Kidney Cancer Research Alliance Research Grant, Simmons Comprehensive Cancer Center (SCCC) Early-Stage Clinical Investigator Award, and Dedman Scholar Award. Research reported herein was supported by the Simmons Cancer Center's Tissue Management Shared Resource and the National Cancer Institute of the National Institutes of Health (grant No. P30 CA142543).

Conflict of interest statement

No potential conflicts of interest are disclosed.

Acknowledgments

We thank Sepeadeh Radpour, MA, MS, PhD, Scientific Research Writer/Editor, Department of Radiation Oncology, UT Southwestern Medical Center, for assistance with manuscript editing and Kaitlyn Marroquin, MS, for assistance with construction of the schematic.

Author contributions

Conceptualized and wrote the manuscript: Soo Lee and Xiaosong Meng.
Performed experiments and collected the data: Soo Lee, Joathan Balcazar, and Karla Davis.
Performed histopathological analysis of tissue staining: Payal Kapur.
Assisted with running of analytic tools: Rey-Chen Pong.
Reviewed and refined the manuscript: Jer-Tsong Hsieh and Xiaosong Meng.

Data availability statement

The datasets used and/or analyzed during the current study are available from the corresponding author upon reasonable request.

References

1. Shin K, Fogg VC, Margolis B. Tight junctions and cell polarity. Annu Rev Cell Dev Biol. 2006; 22: 207-35.
2. Etemad-Moghadam B, Guo S, Kemphues KJ. Asymmetrically distributed PAR-3 protein contributes to cell polarity and spindle alignment in early C. elegans embryos. Cell. 1995; 83: 743-52.
3. Watts JL, Etemad-Moghadam B, Guo S, Boyd L, Draper BW, Mello CC, et al. Par-6, a gene involved in the establishment of asymmetry in early C. elegans embryos, mediates the asymmetric localization of PAR-3. Development. 1996; 122: 3133-40.
4. Macara IG, McCaffrey L. Cell polarity in morphogenesis and metastasis. Philos Trans R Soc Lond B Biol Sci. 2013; 368: 20130012.
5. Gao L, Macara IG, Joberty G. Multiple splice variants of Par3 and of a novel related gene, Par3L, produce proteins with different binding properties. Gene. 2002; 294: 99-107.
6. Le LTM, Drakulic S, Nyengaard JR, Golas MM, Sander B. Structural organization of human full-length PAR3 and the aPKC-PAR6 complex. Mol Biotechnol. 2022; 64: 1319-27.
7. Traweger A, Wiggin G, Taylor L, Tate SA, Metalnikov P, Pawson T. Protein phosphatase 1 regulates the phosphorylation state of the polarity scaffold Par-3. Proc Natl Acad Sci U S A. 2008; 105: 10402-7.
8. Wu H, Feng W, Chen J, Chan LN, Huang S, Zhang M. PDZ domains of Par-3 as potential phosphoinositide signaling integrators. Mol Cell. 2007; 28: 886-98.
9. Zhou PJ, Xue W, Peng J, Wang Y, Wei L, Yang Z, et al. Elevated expression of Par3 promotes prostate cancer metastasis by forming a Par3/aPKC/KIBRA complex and inactivating the hippo pathway. J Exp Clin Cancer Res. 2017; 36: 139.
10. Zhang X, Liu L, Deng X, Li D, Cai H, Ma Y, et al. MicroRNA 483-3p targets Pard3 to potentiate TGF-β1-induced cell migration, invasion, and epithelial-mesenchymal transition in anaplastic thyroid cancer cells. Oncogene. 2019; 38: 699-715.
11. Song T, Tian X, Kai F, Ke J, Wei Z, Jing-Song L, et al. Loss of Par3 promotes lung adenocarcinoma metastasis through 14-3-3ζ protein. Oncotarget. 2016; 7: 64260-73.
12. Guo X, Wang M, Zhao Y, Wang X, Shen M, Zhu F, et al. Par3 regulates invasion of pancreatic cancer cells via interaction with Tiam1. Clin Exp Med. 2016; 16: 357-65.
13. McCaffrey LM, Montalbano J, Mihai C, Macara IG. Loss of the Par3 polarity protein promotes breast tumorigenesis and metastasis. Cancer Cell. 2012; 22: 601-14.
14. Zhou PJ, Wang X, An N, Wei L, Zhang L, Huang X, et al. Loss of Par3 promotes prostatic tumorigenesis by enhancing cell growth and changing cell division modes. Oncogene. 2019; 38: 2192-205.
15. Nakamura H, Nagasaka K, Kawana K, Taguchi A, Uehara Y, Yoshida M, et al. Expression of Par3 polarity protein correlates with poor prognosis in ovarian cancer. BMC Cancer. 2016; 16: 897.
16. Li S, Huang J, Yang F, Zeng H, Tong Y, Li K. High expression of PARD3 predicts poor prognosis in hepatocellular carcinoma. Sci Rep. 2021; 11: 11078.
17. Lv T, Xu J, Yuan H, Wang J, Jiang X. Dual function of Par3 in tumorigenesis. Front Oncol. 2022; 12: 915957.
18. Li T, Liu X, Jiang Q, Lei X, Liu D. High expression of partitioning defective 3-like protein is associated with malignancy in colorectal cancer. Tumour Biol. 2017; 39: 1010428317698393.
19. Jan YJ, Ko BS, Liu TA, Wu YM, Liang SM, Chen SC, et al. Expression of partitioning defective 3 (Par-3) for predicting extrahepatic metastasis and survival with hepatocellular carcinoma. Int J Mol Sci. 2013; 14: 1684-97.
20. Xue B, Krishnamurthy K, Allred DC, Muthuswamy SK. Loss of Par3 promotes breast cancer metastasis by compromising cell-cell cohesion. Nat Cell Biol. 2013; 15: 189-200.
21. Wang S, Cai J, Zhang S, Dong M, Zhang L, Xu Y, et al. Loss of polarity protein Par3, via transcription factor snail, promotes bladder cancer metastasis. Cancer Sci. 2021; 112: 2625-41.
22. Dadras MS, Caja L, Mezheyeuski A, Liu S, Gelabert C, Gomez-Puerto MC, et al. The polarity protein Par3 coordinates positively

self-renewal and negatively invasiveness in glioblastoma. Cell Death Dis. 2021; 12: 932.
23. Dugay F, Le Goff X, Rioux-Leclerq N, Chesnel F, Jouan F, Henry C, et al. Overexpression of the polarity protein PAR-3 in clear cell renal cell carcinoma is associated with poor prognosis. Int J Cancer. 2014; 134: 2051-60.
24. Pei T, Li Y, Wang J, Wang H, Liang Y, Shi H, et al. YAP is a critical oncogene in human cholangiocarcinoma. Oncotarget. 2015; 6: 17206-20.
25. Ortega A, Vera I, Diaz MP, Navarro C, Rojas M, Torres W, et al. The YAP/TAZ signaling pathway in the tumor microenvironment and carcinogenesis: current knowledge and therapeutic promises. Int J Mol Sci. 2021; 23: 430.
26. Yamaguchi H, Taouk GM. A potential role of YAP/TAZ in the interplay between metastasis and metabolic alterations. Front Oncol. 2020; 10: 928.
27. Lamar JM, Stern P, Liu H, Schindler JW, Jiang ZG, Hynes RO. The Hippo pathway target, YAP, promotes metastasis through its TEAD-interaction domain. Proc Natl Acad Sci U S A. 2012; 109: E2441-50.
28. Zhang P, Wang S, Wang S, Qiao J, Zhang L, Zhang Z, et al. Dual function of partitioning-defective 3 in the regulation of YAP phosphorylation and activation. Cell Discov. 2016; 2: 16021.
29. Zou R, Xu Y, Feng Y, Shen M, Yuan F, Yuan Y. YAP nuclear-cytoplasmic translocation is regulated by mechanical signaling, protein modification, and metabolism. Cell Biol Int. 2020; 44: 1416-25.
30. Cai X, Wang KC, Meng Z. Mechanoregulation of YAP and TAZ in cellular homeostasis and disease progression. Front Cell Dev Biol. 2021; 9: 673599.
31. Werneburg N, Gores GJ, Smoot RL. The Hippo pathway and YAP signaling: emerging concepts in regulation, signaling, and experimental targeting strategies with implications for hepatobiliary malignancies. Gene Expr. 2020; 20: 67-74.
32. Sugihara T, Werneburg NW, Hernandez MC, Yang L, Kabashima A, Hirsova P, et al. YAP tyrosine phosphorylation and nuclear localization in cholangiocarcinoma cells are regulated by LCK and independent of LATS activity. Mol Cancer Res. 2018; 16: 1556-67.
33. Shimomura T, Miyamura N, Hata S, Miura R, Hirayama J, Nishina H. The PDZ-binding motif of Yes-associated protein is required for its co-activation of TEAD-mediated CTGF transcription and oncogenic cell transforming activity. Biochem Biophys Res Commun. 2014; 443: 917-23.
34. Du B, Chong Y, Jiang X, Yu M, Lo UG, Dang A, et al. Hyperfluorescence imaging of kidney cancer enabled by renal secretion pathway dependent efflux transport. Angew Chem Int Ed Engl. 2021; 60: 351-9.
35. Bao JM, Dang Q, Lin CJ, Lo UG, Feldkoren B, Dang A, et al. SPARC is a key mediator of TGF-β-induced renal cancer metastasis. J Cell Physiol. 2021; 236: 1926-38.
36. Meng X, Maurel P, Lam I, Heffernan C, Stiffler MA, McBeath G, et al. Necl-4/Cadm4 recruits Par-3 to the Schwann cell adaxonal membrane. Glia. 2019; 67: 884-95.
37. Benton R, St Johnston D. Drosophila PAR-1 and 14-3-3 inhibit Bazooka/PAR-3 to establish complementary cortical domains in polarized cells. Cell. 2003; 115: 691-704.
38. Zhao C, Zeng C, Ye S, Dai X, He Q, Yang B, et al. Yes-associated protein (YAP) and transcriptional coactivator with a PDZ-binding motif (TAZ): a nexus between hypoxia and cancer. Acta Pharm Sin B. 2020; 10: 947-60.
39. Zen K, Yasui K, Gen Y, Dohi O, Wakabayashi N, Mitsufuji S, et al. Defective expression of polarity protein PAR-3 gene (PARD3) in esophageal squamous cell carcinoma. Oncogene. 2009; 28: 2910-8.
40. Li J, Xu H, Wang Q, Fu P, Huang T, Anas O, et al. Pard3 suppresses glioma invasion by regulating RhoA through atypical protein kinase C/NF-κB signaling. Cancer Med. 2019; 8: 2288-302.
41. Zhao Y, Yao D, Li Y, Zhang S, Tao Z, Zhang L, et al. Loss of polarity protein Par3 is mediated by transcription factor Sp1 in breast cancer. Biochem Biophys Res Commun. 2021; 561: 172-9.
42. Koinis F, Chantzara E, Samarinas M, Xagara A, Kratiras Z, Leontopoulou V, et al. Emerging role of YAP and the Hippo pathway in prostate cancer. Biomedicines. 2022; 10: 2834.
43. Lv XB, Liu CY, Wang Z, Sun YP, Xiong Y, Lei QY, et al. PARD3 induces TAZ activation and cell growth by promoting LATS1 and PP1 interaction. EMBO Rep. 2015; 16: 975-85.
44. Jia Y, Li HY, Wang J, Wang Y, Zhang P, Ma N, et al. Phosphorylation of 14-3-3ζ links yap transcriptional activation to hypoxic glycolysis for tumorigenesis. Oncogenesis. 2019; 8: 31.
45. Wang L, Wang L, Zhang H, Lu J, Zhang Z, Wu H, et al. AREG mediates the epithelial-mesenchymal transition in pancreatic cancer cells via the EGFR/ERK/NF-κB signalling pathway. Oncol Rep. 2020; 43: 1558-68.
46. Diskul-Na-Ayudthaya P, Bae SJ, Bae YU, Van NT, Kim W, Ryu S. ANKRD1 promotes breast cancer metastasis by activating NF-κB-MAGE-A6 pathway. Cancers (Basel). 2024; 16: 3306.
47. Huang YT, Lan Q, Lorusso G, Duffey N, Rüegg C. The matricellular protein CYR61 promotes breast cancer lung metastasis by facilitating tumor cell extravasation and suppressing anoikis. Oncotarget. 2017; 8: 9200-15.
48. Zhu X, Zhong J, Zhao Z, Sheng J, Wang J, Liu J, et al. Epithelial derived CTGF promotes breast tumor progression via inducing EMT and collagen I fibers deposition. Oncotarget. 2015; 6: 25320-38.

Cite this article as: Lee S, Balcazar J, Davis K, Pong R, Hsieh J, Kapur P, et al. The polarity protein Par3 enhances renal cell carcinoma metastasis *via* YAP/TAZ activation. Cancer Biol Med. 2025; 22: 812-831. doi: 10.20892/j.issn.2095-3941.2024.0297